

Reactive Micromixing Eliminates Fouling and Concentration Polarization in Reverse Osmosis Membranes

Rajarshi Guha¹, Boya Xiong², Michael Geitner¹, Tevin Moore¹, Thomas K. Wood^{1,3}, Darrell Velegol¹, Manish Kumar^{1,2,4}*

¹Department of Chemical Engineering, The Pennsylvania State University, University Park, PA 16802, United States

²Department of Civil and Environmental Engineering, The Pennsylvania State University, University Park, PA 16802, United States

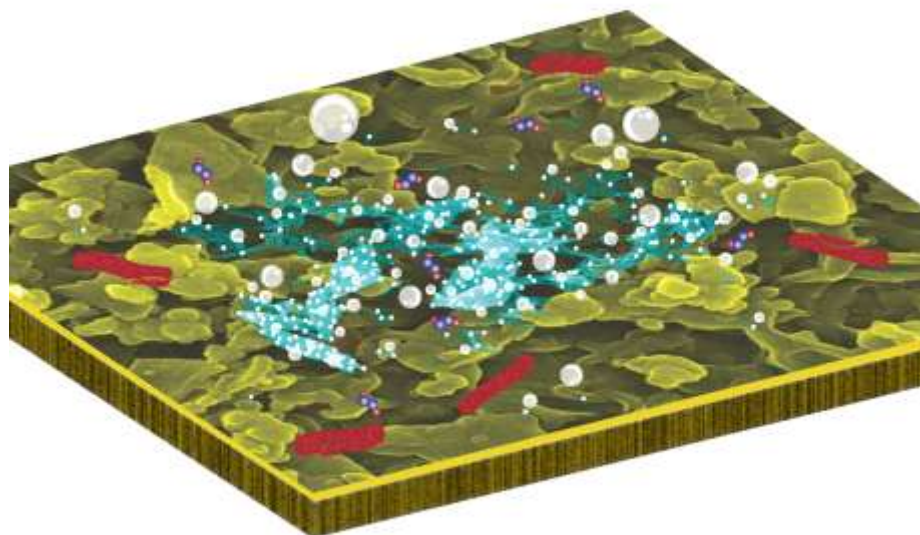
³Department of Biochemistry and Molecular Biology, The Pennsylvania State University, University Park, PA 16802, United States

⁴Department of Biomedical Engineering, The Pennsylvania State University, University Park, PA 16802, United States

***Corresponding Author.** To whom correspondence should be addressed: 43 Greenberg (Chemical Engineering) Laboratory, The Pennsylvania State University, and University Park, PA 16802. Phone: (814) 865-7519. Fax: (814) 865-7519. Email: manish.kumar@psu.edu

ABSTRACT

Reverse osmosis and nanofiltration membranes are used for desalination, wastewater reuse, and industrial water recovery but suffer from high-energy usage during operation. High-energy usage results from membrane fouling and concentration polarization (CP). Fouling is the time dependent deposition of organic macromolecules and particles, as well as the growth of bacterial biofilms on membranes. CP is the accumulation of rejected solutes on the membrane, which reduces the driving force for filtration. We demonstrate a simple, nanoparticle-based, *in situ* approach of inducing chemical reaction-based micromixing on the membrane surface that can simultaneously eliminate fouling and CP. Commercial desalination membrane surfaces were modified with the bioinspired adhesive polymer, polydopamine, and catalytic metal oxide nanoparticles (CuO or MnO₂) were grown and anchored to its surface. This modified membrane catalyzed the degradation of hydrogen peroxide pulse-injected into the feed solution at low concentrations (2-7 mM). The oxygen molecules and hydroxyl radicals generated degraded organic matter and efficiently prevented particle and cell deposition through bubble-generated mixing while causing no observable membrane damage. The reaction generated convection also enhanced solute back diffusion mass transfer coefficients by more than an order of magnitude, resulting in near-complete elimination of CP. Our preliminary results also indicate control of *E. coli* biofilm using the immobilized CuO nanoparticles.

Graphical abstract

KEYWORDS: reverse osmosis membranes, fouling, concentration polarization, metal oxide nanoparticles, H_2O_2 , mass transfer coefficients.

1. INTRODUCTION

Global water scarcity is being progressively exacerbated by population growth, economic development, pollution, and climate change. It is expected that our accessible water supplies will have to be increased by 40 % over current levels to close the water supply and demand gap by 2030 [1]. Developing untapped lower-quality water sources, including seawater, brackish water and recycled wastewater, is therefore critical to global water sustainability. Membrane

separations, especially high-pressure membrane processes such as reverse osmosis (RO) and nanofiltration (NF), have become most used technologies for energy-efficient utilization of these alternative water sources [2,3]. Despite large advances in membrane materials development [4], high pressure membrane processes suffer from performance deterioration of membranes and high energy consumption [5,6]. Two persistent issues in these membrane systems that increase energy consumption and contribute to increased operational costs are: 1) concentration polarization (CP) where solute build up on the membrane surface causes enhanced osmotic pressure and reduces the driving force for transport of water while at the same time, increasing the driving force for passage of contaminants, and 2) fouling, where colloidal particles, organic matter, and microbes deposit on membranes leading to increase in total membrane resistance and observable performance deterioration in these systems. Indeed, Elimelech and Phillip have recently argued that the efficiency of current membrane materials is approaching its thermodynamic limit for seawater desalination and the further gains in efficiency can only be achieved by improving system and operational design including better pretreatment, minimization of CP, and mitigation of fouling [6]. CP development is almost instantaneous and is exacerbated by deposited foulants that can trap dissolved solutes. However, mitigation of CP has been overlooked as an area of research and development in recent years despite its significant contribution to osmotic pressure increase and flux decline in high pressure membrane separation. Currently commercialized solutions for CP mitigation require a redesign of current membrane infrastructure with rotating or vibrating modules [7]. We propose a simple technique to address both CP and fouling challenges simultaneously, which can be implemented in existing membrane infrastructure easily (**Fig. 1**) while having the potential to reduce energy consumption by over 30 %, a substantial number given the current installed capacity of over 10 billion gallons

per day of reverse osmosis [8] and the projected 10.5% growth per annum over the next decade [9].

Several technologies, including those based on nanoparticle incorporation into the active layer of the membrane have attempted to address fouling by designing smoother surfaces [10], enhancing membrane hydrophilicity [11], altering surface charge [12] or using a polymer grafted membrane surface [13] to repel foulants by inherent volume exclusion - steric repulsion mechanisms [14]. However, few mitigation methods have been found to be effective for long term fouling prevention and moreover, prevent only specific types of membrane fouling. Additionally, in all membrane cleaning processes, operation needs to be stopped before the backwash begins for microfiltration/ ultrafiltration and chemical cleaning or direct osmosis cleaning begins for RO or NF [15]. These intermittent cleaning steps lead to a decrease in overall productivity and increase in cost of operation. Therefore, to save energy and decrease overall costs, self-cleaning membranes which can address multiple foulants without hindering regular operation could be a general and effective solution for fouling mitigation.

A focus of previous research was on fabrication of hybrid and composite membranes to actively reduce bacterial attachment on the membrane surface either by photocatalytic or electrolytic routes [16,17]. In one of the earliest studies, Park *et al.* fabricated stable surface attached titania (TiO_2)-TFC (thin film composite) hybrid membranes which upon exposure to UV light reduced bacterial attachment and also reduced overall flux decline by 50% [16]. Nitto Denko has developed composite semipermeable membranes with a thin skin layer of polyvinyl alcohol embedding Ag or TiO_2 nanoparticles [18–20]. Such membranes impart higher hydrophilicity and decrease microbial adhesion. In a recent study, Ray *et al.* demonstrated photo-thermal composite membrane activation and its effectiveness in mitigating different foulants

found commonly in RO systems [21]. Electrolytic approaches which are driven by external power source, require design of nano-composite TFC membranes with carbon nanotubes which render it electrically conductive [17] have also been shown to be effective. Such membranes were shown to recover flux lost due to biofouling after application of an alternating voltage across membrane and cross flow flushing. A similar approach was implemented to remove inorganic scaling on such conductive RO membranes and recover flux by applying higher DC voltage to generate H^+ ions near membrane surface and subsequent dissolution/removal of scaling materials [22]. Dudchenko *et al.* reported organic fouling mitigation using such conductive membranes in ultrafiltration systems [23]. Jing *et al.* reported chemical free electrochemical regeneration of ceramic ultrafiltration membranes and proposed hydroxyl radicals and bubble induced shearing as possible mechanisms of organic foulant removal.[24] from membrane surface. Chesters *et al.* reported external bubble enhanced cleaning of RO membranes with commercial effervescent reagents instead of traditional acid and base cleaning techniques [25]. However, applications of these strategies are either achieved by impeding operation, equivalent to cleaning steps [15] or continuously applying higher voltages or magnetic fields with added infrastructure [26] and expensive membrane architectures. Moreover, the flux recoveries of such approaches have not always been efficient, mostly lasting for only few hours and not comprehensively demonstrated with different foulants.

Polydopamine coatings on membranes surface have reported to yield superior resistance to fouling by increasing surface hydrophilicity and by enabling further surface functionalization [27]. This scalable approach imparts only insignificant mass transfer resistance to flux [28] and therefore, can be used as a starting point for developing fouling elimination strategies.

Polydopamine functionalized membranes with polyvinyl pyrrolidone and Iodine were demonstrated to enhance rejection of oily wastewater and eliminate microbial attachments [29]. Polydopamine was also reported to strongly bind TiO_2 nanoparticles compared to other commonly used surface modification techniques and also improved salt rejection performance of the TFC membrane [30]. Non-covalent co-ordinate complexation between metal oxide and catechol groups of PDA ensures strong adhesion and remarkable stability under shear of metal oxide-PDA films [30,31]. Tang *et al.* demonstrated direct synthesis of silver nanoparticles on the membrane surface using the reductive properties of polydopamine, which completely eliminated bacterial attachment while maintaining significantly lower leaching rates of Ag^+ ions to the surroundings [32]. Polydopamine surface functionalization has been limited to applications such as polymer grafting induced fouling prevention and biofouling reduction. There is no report so far on nanoparticle catalysis induced fouling elimination and flux recovery.

We hypothesized that under cross flow operating conditions, when a foulant layer is formed, *in-situ* generation of molecular oxygen “bubbles” and their subsequent release and/or bursting near the membrane surface impart convective disturbances in the dense cake layer (**Fig. 1**). This convective mechanism leads to disruption of the cake layer, increase in porosity, and finally, dispersion of the particulate matter. Additionally, bubbles can generate jet flows and oscillating wall motion to impart cleaning action (**Supplementary Information**). We have shown here that with polydopamine (PDA) – metal oxide nanoparticle (NP) surface coated composite RO membranes, fouling can be completely reversed upon pulse injection of ppm levels of H_2O_2 in the feed without hindering or stopping membrane permeation. H_2O_2 is catalytically decomposed by metal oxide nanoparticles on the PDA surface to molecular oxygen and water. Use of H_2O_2 as a membrane cleaning solution is already in industrial practice and is

recommended at 0.2% (~56 mM) [33]. PDA is also a strong free radical scavenger and forms a protective barrier [34] over the underlying polyamide layer to protect it from excess free radicals generated by the peroxide. Additionally, polydopamine layer is very stable and high concentration (30%) of H_2O_2 is needed to remove it [35]. For certain chelating and catalytic foulants, such as humic acids, this reaction approach substantially perturbed the concentration boundary layer leading to flux increase beyond the baseline initial flux level due to mitigation and, in some cases, elimination of concentration polarization. At higher operating fluxes and cross flow velocities, an order of magnitude enhancement of solute back diffusion mass transfer coefficients held the CP modulus (a measure of the extent of CP) to very low values, equivalent to pressurizing pure water through the membrane. Such H_2O_2 injections did not change intrinsic membrane permeability and salt rejection over repeated use, confirming the robustness of this approach. Overall, this simple approach presents a potentially scalable solution to RO fouling mitigation and perhaps even reversal in large-scale industrial settings. The application of this approach was also demonstrated to result in decreased bacterial attachment and biofilm formation on membranes.

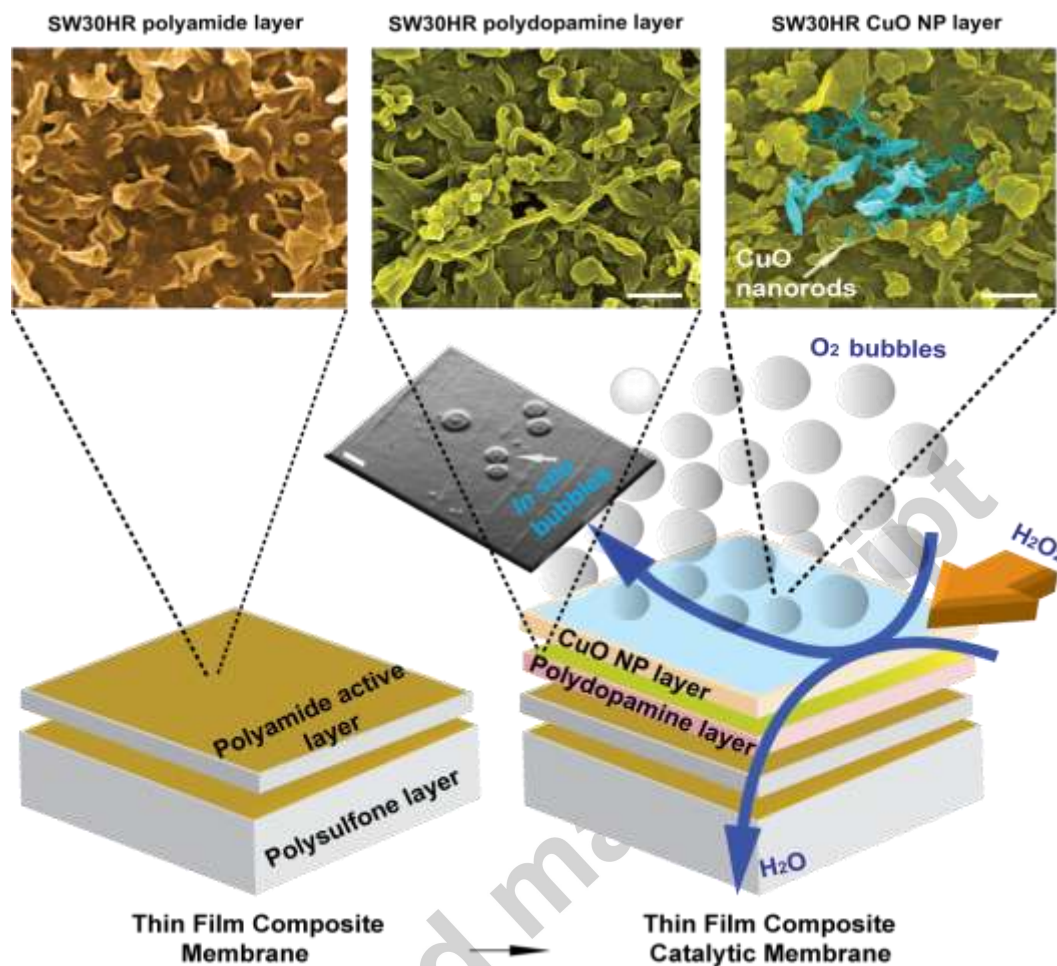


Fig 1. Schematic of catalytic/ reactive membrane assembly and realization of mechanism of action. The active polyamide layer of thin film composite membrane was coated with polydopamine. Cupric oxide (CuO) nanoparticles were thereafter deposited on the polydopamine layer. Hydrogen peroxide (H_2O_2) was added to this membrane which on dissociation to molecular oxygen and water, generated *in situ* bubbles on the membrane surface sweeping away deposited foulants and disrupting concentration polarization. The SEM images have scale bars of 500 nm and the *in situ* bubbles image has scale bar of 150 μm .

2. MATERIALS AND METHODS

2.1. Polydopamine coating and anchoring of CuO and MnO_2 nanoparticles on membrane surfaces

Flat sheet seawater RO membranes (DOW SW30HR) and NF membranes (NF90) were obtained from Dow Water and Process Solutions (DWPS) and were used for colloidal/organic fouling and biofilm control experiments, respectively. Dopamine hydrochloride (Sigma, lot# BCBP6519V) was polymerized in 10 mM Tris-HCl buffer maintained at pH ~ 8.5 and coated on respective thin film composite membranes (TFC) under continuous rocking conditions (**Supplementary Information**). CuO nanoparticles were prepared at room temperature using drop-by-drop addition of NaOH to a $\text{Cu}(\text{NO}_3)_2 \cdot 2\text{H}_2\text{O}$ (Strem Chemicals, lot# 21842300) precursor solution in ultrapure water (Barnstead Nanopure, Model 7146, 18.2 M Ω -cm) (**Supplementary Information**) [36]. The modified membranes are referred to as 8 ppm CuO/PDA or 80 ppm CuO/PDA based on precursor concentrations (**Supplementary Table S1**). A schematic of the surface-active catalytic membrane with added polydopamine and metal oxide layers is shown in **Fig. 1**, and micrographs of resulting membranes and nanoparticles are shown in **Fig. 2**. MnO_2 nanoparticles were also synthesized and loaded on RO membranes following a similar drop-by-drop method (**Supplementary Information**).

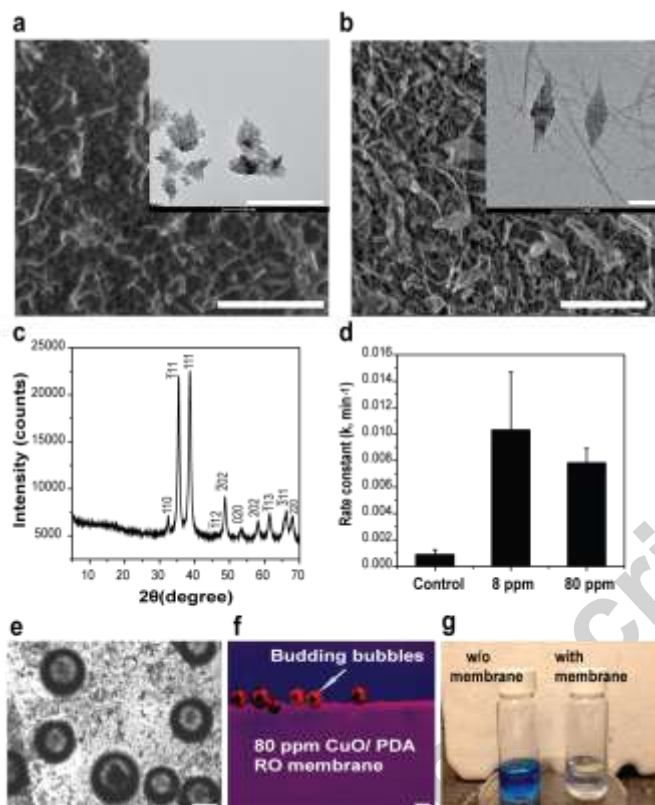


Fig 2. Catalytic/ reactive membrane characterization using SEM, XRD and methylene blue decolorization reaction. (a) SEM image of a 8 ppm CuO/PDA membrane with the inset showing TEM image of CuO nanoflakes. The scale bar represents 1 μm for SEM and 200 nm for TEM. (b) 80 ppm CuO/PDA membrane with inset showing TEM image of CuO nanorods. The scale bar represents 1 μm for SEM and 200 nm for TEM, (c) XRD analysis of CuO nanoparticles (nanorods) indicate the presence of monoclinic tenorite. (d) Methylene blue degradation kinetics using different CuO/PDA membranes. The reaction rates were almost equivalent, except 80 ppm membranes have slightly lower activity than 8 ppm membranes (**Supplementary Table S1**). (e) Microbubble formation from CuO nanorods in presence of H_2O_2 as observed under bright field microscopy. The scale bars are 100 μm . (f) False color image of *in situ* bubble evolution from 80 ppm membrane surface in 3% H_2O_2 solution under static conditions. The bubbles are dyed with Rhodamine 6G for imaging, and the scale bar is 150 μm (details in **Supplementary Information**). (g) Methylene blue was decolorized in the presence of 2 cm^2 surface area of 8 ppm CuO/PDA membrane and 3% H_2O_2 .

2.2. Nanoparticle characterization using XRD, SEM and TEM

CuO nanoparticles were characterized using X-Ray Diffraction (XRD) with a 2θ range of 5 - 70° at the Cu-K α wavelength. All the highlighted peaks (**Fig. 2c**) can be indexed to the

crystalline monoclinic tenorite phase of CuO (Powder Diffraction File (PDF-2) entry: 48-1548) [37]. The unmodified and modified membranes were characterized using scanning electron microscopy (FEI Helios NanoLab 660 or FEI NanoSEM 630) for surface morphology (**Fig. 1, Fig. 2 and Supplementary Fig. S1**). The CuO nanoparticles were also separately synthesized and imaged using an FEI Techai G2 Spirit Bio Twin transmission electron microscope (TEM) operated at 80 kV (**Fig. 2a and b, inset**).

2.3. Kinetic evaluation of membrane performance using methylene blue decolorization

Bubble generation on the membrane surface was visualized *in situ* using bright field as well as fluorescence microscopy (**Fig. 2e-f**). Rhodamine 6G was used to visualize the bubbles budding out from the active surface of the RO membrane in presence of H₂O₂ (**Fig. 2f and Supplementary Information**). Catalytic properties were analysed using a model batch reaction - methylene blue decolorization (**Fig. 2g**). For a given CuO/PDA membrane, three independent 1 cm x 2 cm randomly cut pieces were used to degrade methylene blue (12 mg/L) with 3% H₂O₂ (Fisher Scientific, lot# 146706) in 5 ml solution volume (**Supplementary Video 1**). Absorbance was measured at different time points using UV-VIS spectrophotometry (Thermo Scientific Evolution 201) at a wavelength of 667 nm. A first order reaction kinetic rate equation was fitted to this data to obtain the rate constant and thereby, catalytic activity of the membrane. Catalytic activities of MnO₂/PDA membranes were weaker than CuO/PDA membranes as evident from methylene blue decolorization test (**Supplementary Fig. S2a**). The rate constant of 8 ppm MnO₂/ PDA membrane was ~ 45% lower than 8 ppm CuO/PDA membrane.

2.4. Probing of hydroxyl radical generation during H₂O₂ dissociation

In order to probe generation of hydroxyl radicals ($\text{OH}\cdot$), we conducted batch reactions in 5 ml solution volumes containing different concentrations of H_2O_2 and CuO nanoparticles in solution or using 1 cm x 2 cm randomly cut pieces of 80 ppm CuO/PDA membranes (**Supplementary Fig. S2b**) prepared as described in section 2.3. We used around 0.01 ppm CuO nanoparticles in 5 ml volume, which was near to the estimated amount of CuO nanoparticles on 2 cm² membrane surface. 2 mM terephthalic acid (lot#MKCC2903) was used as $\text{OH}\cdot$ probe in the reaction. 5 mM NaOH was used in all batch reactions in order to dissolve terephthalic acid. The reactions were performed in triplicate under vigorous stirring for 24 h and the reaction products were collected after filtering through a 200 nm disc filter. 2-hydroxyterephthalic acid (lot# MKBZ2972V) standards were prepared in 5 mM NaOH in order to obtain the calibration for $\text{OH}\cdot$. 200 μL of standards and reaction products were loaded on a 96-well plate and was analysed using a microplate reader (SpectraMax i3, Molecular Devices) at 310 nm/425 nm excitation/emission.[38]

2.5. Cross flow RO system for run time evaluation of membrane performance

Colloidal silica particles of 80 nm mean diameter, Snowtex-ZL (lot# 250612), was supplied by Nissan Chemical America Corporation (Houston, TX) and humic acid (lot#BCBG7429V) was obtained from Aldrich (St. Louis, MO). These have been extensively used in previous work for colloidal [5,39] and organic fouling [40] experiments as standard RO foulants for laboratory evaluation. NaCl (lot#49H0264) was purchased from Sigma-Aldrich and 20 mM NaCl concentration was used throughout all fouling experiments. A constant pressure bench scale cross flow RO system equipped with an Osmonics[®] SEPA CF membrane cell of 138 cm² filtration area (Sterlitech corp., Kent, WA) was used for colloidal and organic fouling experiments. The CuO/PDA RO membranes were compacted for 24 h in DI water and then

conditioned with 20 mM NaCl for further 12 h before charging foulants (0.017% silica nanoparticles for colloidal fouling and 50 ppm HA for organic fouling). The fouling (4 L feed volume) experiment was further continued for another 24 – 48 h before addition of a 60 – 240 ppm H₂O₂ pulse into the feed tank. The pulse injection of H₂O₂ into the feed tank took ~1 s and it was mixed uniformly with the help of a feed tank overhead stirrer (IKA RW 20). Concentration polarization experiments with 80-ppm CuO/PDA membranes were performed with flux measurements for 2-6 h at different NaCl feed concentrations (0-250 mM range) and 240 ppm (~7 mM) H₂O₂ injection at each NaCl concentration (**Supplementary Information**).

2.6. Biofilm control experiment with *E. coli* in stirred cell setup

Biofilm experiments were performed with *E. coli* as a model organism in an Advantec MFS UHP-76 (Dublin, CA, USA) stirred cells with an effective membrane area of 35.3 cm². Wild type red fluorescent protein (rfp) incorporated *E. coli* (*E. coli* TG1/pBdcAE50Q-*rfp-lasR*) was used as a model organism for biofilm development as in a recent study conducted by our group [41]. Such biofilms were developed on NF90 membranes over a 24 h time period using M9-0.4% glucose (M9G) medium with chloramphenicol (Cm, 300 µg/ml) antibiotic for sustaining *rfp* plasmids. NF90 membrane was particularly used in this preliminary biofilm study to compare the effectiveness and obtain an estimate of flux improvement particularly in comparison with previous study [41] where an identical evaluation technique was employed. A laser scanning confocal microscope TCS SP5 (Leica Microsystem, Wetzlar, Germany) equipped with a 63x/1.4 oil objective lens, a 488/514 nm double dichoric lens with the ability to scan from 550 nm to 650 nm was used to visualize the biofilms. H₂O₂ addition to this system was only performed after a 24 h growth period and then the stirred cell was incubated for 10 minutes at room temperature.

3. RESULTS AND DISCUSSION

3.1. Catalytic metal oxide nanoparticles can be successfully grown and immobilized on commercial NF/RO membranes.

A schematic of the surface-active catalytic membrane with added polydopamine and metal oxide layers is shown in **Fig. 1**, and micrographs of resulting membranes and nanoparticles are shown in **Fig. 2** and **Supplementary Fig. S1**. CuO nanoparticles were synthesized *in situ* on commercial membrane surfaces using a drop-by-drop method reported before with modifications (**Supplementary Information**). These nanoparticles were characterized using x-ray diffraction (XRD) as discussed in section 2.2. We find that the membrane surface tethered catalysts follow 1st order kinetics in a methylene blue decolorization reaction (**Fig. 2d**). The evolution of the bubbles, after contact with H₂O₂, from the CuO nanoparticles and also from the CuO anchored SW30HR desalination membranes is depicted in **Fig. 2e-2g**. Generation of these molecular O₂ bubbles on the membrane surface can be observed directly during the decomposition of H₂O₂ (**Fig. 2f and Supplementary Video S1**).

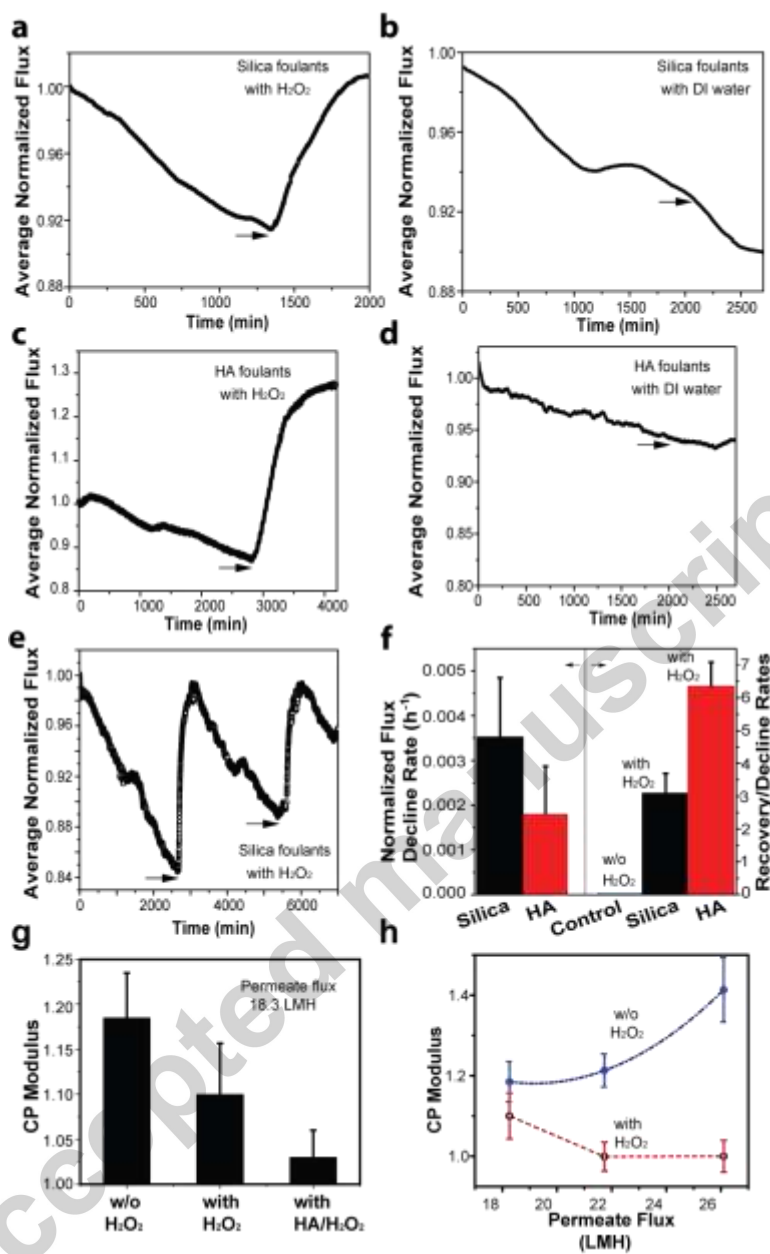


Fig 3. Flux decline was reversed and concentration polarization was significantly diminished *in situ* with the use of catalytic/ reactive membrane and pulse addition of H_2O_2 . (a) Flux declined with operation of 8 ppm CuO/ PDA RO membrane at ~18 LMH with the addition of 0.017% silica nanoparticles at 19°C. Substantial flux recovery was seen upon 240 ppm H_2O_2 addition (indicated by the arrow). (b) Flux declined with operation of virgin RO membrane (control) at ~18 LMH, 19°C, with addition of 0.017% silica nanoparticles. However, no flux recovery was seen upon addition of DI water (same volume as H_2O_2). (c) Flux declined with operation of 8 ppm CuO/PDA RO membrane at ~18 LMH, 19°C with addition of 50 ppm humic acid (HA) and rapid flux recovery was seen upon 240 ppm H_2O_2 addition. The recovered flux exceeded prefouling flux due to decrease in concentration polarization. (d) Flux declined with operation of virgin RO membrane at ~18 LMH, 19°C on addition of 50 ppm HA and flux

decline continued (with no flux recovery) with DI water addition (same volume as H₂O₂). **(e)** Repeated flux decline and recovery cycles with 0.017% silica nanoparticles under similar conditions indicate the robustness of the proposed approach. **(f)** Normalized average flux decline rates for silica and HA foulants on the left y-axis and recovery to decline rates' ratios for both silica and HA foulants with control (both silica and HA) on the right y-axis. Flux recovery rates for HA were almost twice that of silica nanoparticles. **(g)** Concentration polarization (indicated by CP modulus) was reduced with H₂O₂ addition due to bubble enhanced mixing and increased mass transfer co-efficients. At relatively lower fluxes, such as at 18.3 LMH, addition of HA further reduced concentration polarization by enhancing the reaction. **(h)** At higher fluxes, addition of H₂O₂ kept the concentration polarization modulus at ~ 1. Such reduction was shown with 80 ppm CuO/PDA modified SW30HR membrane at 18.3 LMH, 21.7 LMH and 26.1 LMH fluxes with and without addition of only 240 ppm H₂O₂ in the feed tank.

3.2. RO flux decline due to colloidal and organic fouling can be completely reversed by pulse addition of ppm levels of H₂O₂ to catalytic membranes.

We observed robust reversal of the flux decline during real time operation of a bench-scale RO system with the catalytic membrane upon addition of H₂O₂ (**Fig. 3**). This effect was observed with both silica colloids as well as humic acids (HA) as model foulants. Specifically, with 18 liters per meters squared per hour (LMH) initial flux, 0.017% silica nanoparticles caused rapid fouling and decreased the normalized flux by 9% in 1300 min. Addition of 240 ppm H₂O₂ increased the flux value to the original prefouling level within 2000 min of operation (**Fig. 3a**). A normalized flux decline rate from fouling, and a flux recovery rate on addition of H₂O₂ was calculated to provide a measure of the real-time fouling reversal effectiveness of the proposed strategy. The average normalized flux decline rate was $0.0035 \pm 0.0013 \text{ h}^{-1}$ and average flux recovery rate on H₂O₂ addition was $0.011 \pm 0.005 \text{ h}^{-1}$ for colloidal silica foulants. Therefore, the flux recovery rate was almost 3 times that of the flux decline rate. The control experiment, performed with only virgin (uncoated) SW30HR RO membranes, showed no observable effect of flux improvement if only DI water was added and it continued to decrease during the course of data collection (**Fig. 3b**). The catalytic approach is robust and also reproducible as shown with

the multiple flux decline and recovery cycles using the same composition of silica foulants and H₂O₂ (**Fig. 3e**). This is also an example of on demand flux decline elimination, since H₂O₂ can be injected at any point of time during the filtration process and the flux would recover rapidly to the pre-fouling level (**Supplementary Fig. S3**).

We propose that the dominant forces on a free bubble, just separated from the surface, are buoyancy and electrostatics, acting toward and away from the membrane, respectively (**Supplementary Information and Supplementary Fig. S4**). These free moving bubbles on membrane surface can cause rapid mixing in the concentration boundary layer by entraining surrounding liquids to develop strong recirculation flows [42]. Additionally, surface attached bubbles can impart adverse pressure gradients to crossflow and may generate recirculation wakes by a phenomenon known as separation bubbles [43]. Apart from this micromixing induced disruption of particle deposition, strong repulsive van der Waals interaction [44,45] of ~8 kT at the electrical double layer length scale in silica foulants-water-O₂ bubble system may contribute as an additional mechanism (**Supplementary Information**).

Humic acid foulants also decreased the flux during standard operation without catalytic action, at a slower rate than silica nanoparticles (**Fig. 3c**). Both CuO/PDA modified membranes and control membranes were fouled at similar rates and DI water addition did not result in flux improvement (**Fig. 3d**). Due to degradation of HA and concomitant micromixing driven enhanced mass transfer near the membrane after H₂O₂ addition, the flux recovered rapidly as in case of CuO/PDA modified membrane. Surprisingly, the normalized flux increased to values greater than 1.0 and this increase was sustained for more than 24 h. During this time period, the foulants were kept dispersed by ongoing reactions and concentration polarization was also mitigated. The average flux decline rate for HA foulants was $0.0018 \pm 0.0010 \text{ h}^{-1}$ and average

flux recovery rate was $0.014 \pm 0.005 \text{ h}^{-1}$ for the same foulants with the catalytic membrane. Therefore, the flux recovery rate for HA was more than 6 times faster than the decline rate and also 30% higher than silica case. This might be attributed to the catalytic effects of HA (**Supplementary Fig. S5**). Since, H_2O_2 decomposition on CuO surface is a Fenton-like process [46], synergistic catalysis of CuO-HA complex can accelerate the reaction rate. Furthermore, HA has been demonstrated to act as an electron shuttle [47] accelerating H_2O_2 decomposition, OH^\cdot radical generation and low molecular weight acid production [48], which might impart cleaning action on membrane surface through local pH changes, reaction induced micromixing [49] and reverse diffusiophoresis [50]. For example, one of the HA degradation products, oxalic acid [51] might be able to develop internal electric fields on membrane surface opposite to NaCl generated one due to faster back diffusion of H^+ ions- generating reverse diffusiophoretic transport of colloidal particles away from the membrane. Such cleaning effects and transport would also result in mitigation of concentration polarization. This is further explored in the next section. Unlike enhanced micromixing in HA case (rate constant of CuO-HA complex $\sim 0.08 \pm 0.02 \text{ min}^{-1}$), the micromixing with colloidal silica foulants (rate constant of 80 ppm CuO/PDA $\sim 0.034 \pm 0.002 \text{ min}^{-1}$) was not strong enough to cause the flux to increase beyond the pre-fouling level due to unreactive, larger, and denser silica particles. In the HA case, the flux recovery rate was observed to depend on concentration of H_2O_2 charged (**Supplementary Fig. S6**). This observation supported our measurements of H_2O_2 concentration dependent generation of OH^\cdot (**Supplementary Figure S2b**) which was reported to be involved in HA degradation reactions [24]. Complete flux decline reversal with HA foulants required a minimum H_2O_2 dosing of 60 ppm under the operating conditions of the experiments conducted (18 LMH initial flux and 50 ppm HA). We show that that 240 ppm H_2O_2 addition could generate $41.9 \pm 4.8 \text{ } \mu\text{M}$ of OH^\cdot per 2

cm² of 80 ppm CuO/PDA membrane area and therefore, degradation of HA and flux recovery would be accelerated (**Supplementary Figure S2b**).

MnO₂ modified membranes (8 ppm) demonstrated slower response on addition of H₂O₂ (**Supplementary Fig. S7**). Since the kinetic rate constant of H₂O₂ dissociation by embedded MnO₂ nanoparticles on PDA modified membranes were lower, the lower flux recovery rates found were expected for both silica and HA foulants. Furthermore, we observed that at 60 ppm H₂O₂ injection, the flux recovery to decline ratio of MnO₂/PDA membranes was only 1.90±0.01 for both silica as well as HA foulants (**Supplementary Fig. S7**). In contrast, at 60 ppm H₂O₂ injection, the flux recovery to decline ratio of CuO/ PDA membranes for HA foulants was 5.8±0.4 (**Supplementary Fig. S6**). Therefore, PDA supported CuO catalysis of H₂O₂ is much more effective than MnO₂ in mitigating RO membrane fouling.

3.3. Concentration polarization can be reduced/eliminated by reactive micromixing in the presence of H₂O₂.

The CuO/PDA membranes were effective in reducing concentration polarization upon addition of H₂O₂. CP is characterized by the concentration polarization modulus (f_{CP}) which is simply the ratio of the concentration of salts in the bulk feed (C_b) solution to that on the membrane surface (C_m) as given by **Eq. (1)** and evaluated using a procedure described in literature (also see **Supplementary Information**) [52]. A f_{CP} of 1.0 indicates complete elimination of concentration polarization.

$$f_{CP} = \frac{C_m}{C_b} \quad (1)$$

At lower fluxes such as 18.3 LMH, a CP modulus of ~ 1.2 was observed with 80 ppm CuO/PDA modified RO membrane at 20 mM NaCl feed concentration (**Fig. 3g**). Addition of 240 ppm H_2O_2 reduced the CP modulus to 1.1 which was further reduced to 1.03 with addition of both 240 ppm H_2O_2 and only 10 ppm HA. HA catalyzed reduction in CP modulus was primarily responsible for flux improvement beyond pre-fouling levels as shown in **Fig. 3c**. At higher fluxes such as at 26.1 LMH, we find that addition of HA (without H_2O_2 addition) increased the CP modulus beyond that expected from just the effect of increasing flux. This is due to HA deposition induced cake enhanced concentration polarization at higher fluxes [53]. In all cases, addition of H_2O_2 substantially reduced concentration polarization (**Fig. 3h**).

To quantify the efficiency of mass transport, we compared the normal back transport mass transfer co-efficient of the solute without any bubble induced micromixing (k_0) with the equivalent bubble enhanced back transport mass transfer co-efficient (k). Both k_0 and k can be estimated using the stagnant film model based on the measured concentration polarization modulus (f_{CP}) and the membrane flux (V_w) [54]. At lower fluxes such as 18.3 LMH ($V_w = 5.08 \mu\text{m/s}$), the CP modulus without any H_2O_2 addition and bubble generation was 1.2 (**Supplementary Table S2**). The solute back diffusion mass transfer co-efficient of NaCl (k_0) in the concentration boundary layer can be estimated from $k_0 \sim V_w / \ln CP = 3.0 \times 10^{-5} \text{ m/s}$. However, with 240 ppm H_2O_2 addition and bubble generation, the CP modulus was reduced to 1.1 at the same flux. Concomitantly, the micromixing enhanced solute back diffusion mass transfer co-efficient of NaCl (k) was increased to $5.34 \times 10^{-5} \text{ m/s}$. At higher fluxes, as shown in **Fig. 3h**, the CP modulus increased without addition of H_2O_2 as expected due to the exponential relationship of CP modulus to flux given by **Eq. (2)**.

$$f_{CP} = \exp\left(\frac{V_w}{k}\right) \quad (2)$$

When H₂O₂ was added in case of fluxes higher than 18.3 LMH, micromixing was highly enhanced and the solute back diffusion mass transfer coefficient increased more than an order of magnitude (**Supplementary Table S2**). With the increase of permeate flux under normal condition, i.e. without any bubble generation, the solute back diffusion mass transfer coefficient reduced due to larger convective drag towards the membrane, leading to higher concentration polarization. However, the bubble enhanced convection generated efficient micromixing to cause $k \gg V_w$ at higher fluxes. This translated into holding the CP modulus at ~ 1 (indicating complete elimination of concentration polarization), perhaps a first with such a simple approach. The ability of membranes to operate at higher fluxes without concentration polarization may be particularly important for high flux membranes such as graphene-based membranes [55], carbon nanotube based membranes, and aquaporin based biomimetic membranes being proposed for desalination and water reuse [56].

3.4. CuO NPs reduces bacterial attachment to the membranes.

Two different CuO nanoparticle loadings (in the form of nanorods) on NF90 membrane were tested to examine the efficacy of these nanorods in combating biofilm formation. Gunawan *et al.* reported a relatively high CuO loading as being required to reduce *E. coli* growth [57]. Therefore, bulk CuO loadings of 8 (0.0027±0.0002 mg/m² Cu) and 80 ppm (0.0065±0.0006 mg/m² Cu) were applied on PDA coated membrane. Leached copper-peptide complex induced reactive oxygen species (ROS) eventually damages the bacterial cell wall [57]. In accordance with this finding, higher loading of CuO (80 ppm) was found to be more effective in preventing

bacterial attachment and controlling biofilm formation (**Fig. 4**). CuO/PDA catalytic membrane generates higher concentrations of OH \cdot which would be advantageous in combating different biofilms. We found ~ 3 fold increase in biofilm formation with only PDA modified membrane over unmodified membranes. This was also previously observed by Cui *et al.* [58]. The increased surface roughness due to PDA coating may be responsible for such enhanced biofilm. The surface hydrophilicity was also increased with the modified membrane (80 ppm CuO/PDA coating) as the mean contact angle was reduced by $\sim 1/3^{\text{rd}}$ (sessile drop mean contact angle measurements for virgin RO membrane was 45 $^{\circ}$ and for 80 ppm CuO/ PDA membrane was 13 $^{\circ}$). This resulted in improved hydration of membrane surface and better contact with cellular biomass in order to facilitate ROS generation. Therefore, the specific biomass (measured in $\mu\text{m}^3/\mu\text{m}^2$) was reduced by 88% and 95% in the 8 ppm and 80 ppm CuO/PDA membranes, respectively, with respect to virgin NF90 membranes (**Fig. 4f**). Surprisingly, we found similar amount of reduced biomass ($\sim 0.1 \mu\text{m}^3/\mu\text{m}^2$) using 80 ppm CuO/PDA membranes as reported by Wood *et al.* with genetically modified *E. coli.* on NF90 membranes [41]. Conforming to this study, we anticipate that $\sim 50\%$ improvement in permeate flux can also be achieved with CuO/PDA membrane, compared to unmodified NF90 membrane. The fold reductions in biofilm biomass (i.e. biomass on virgin NF90/ biomass on modified NF90) were 8.2, 21.2 and 25.0 times in cases of 8 ppm CuO/PDA, 80 ppm CuO/PDA and 240 ppm H $_2$ O $_2$ incubated 80 ppm CuO/PDA membranes, respectively. Overall, such membrane modification approach was efficient in reducing bacterial attachment and biofilm formation with and without H $_2$ O $_2$ addition.

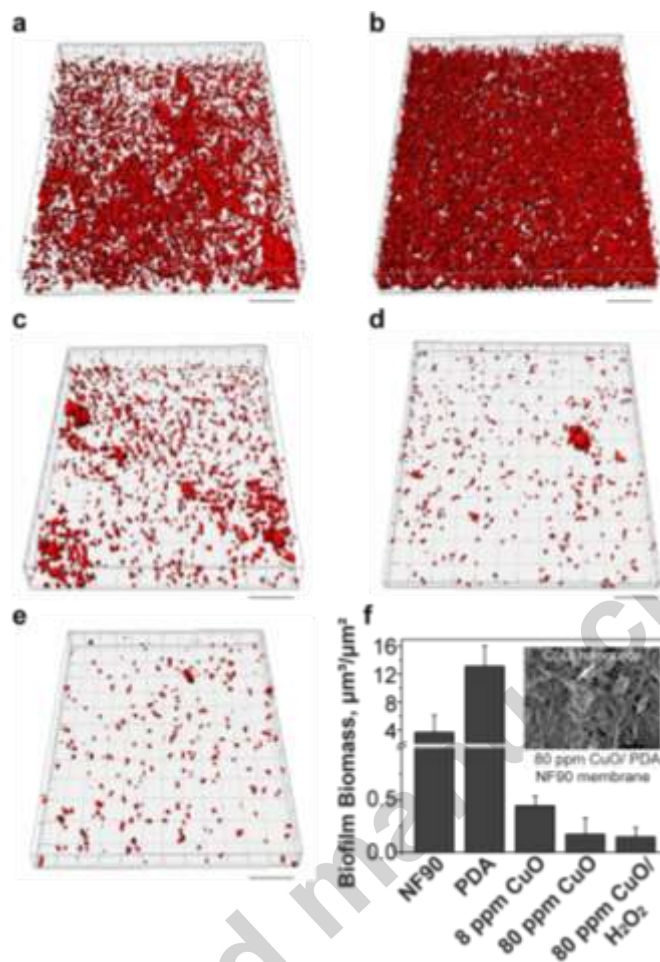


Fig 4. Biofilm control and substantial bacterial attachment reduction can be achieved with the catalytic/ reactive membrane (a) *E. coli* biofilm on virgin/ unmodified NF90 membrane surface. (b) Enhanced *E. coli* biofilm on only PDA coated membrane surface. (c) Reduced *E. coli* biofilm on 8 ppm CuO/ PDA coated NF90 membrane. (d) Further biofilm reduction on 80 ppm CuO/PDA coated NF90 membrane. (e) Biofilm on 80 ppm CuO/PDA coated NF90 membrane after incubation with 240 ppm H₂O₂. The scale bars in (a)-(e) are 20 μm. (f) Comparison of biofilm biomass for different membranes showed that addition of 240 ppm H₂O₂ on 80 ppm CuO/PDA membrane decreased bacterial attachment to the highest extent. However, this was only marginally higher in biofilm reduction than 80 ppm CuO/PDA membranes. The error bars are standard deviations of at least N = 5 membrane samples spanning 3 independent colonies. The inset SEM image corresponds to CuO nanorods on PDA coated membrane surface, which act as anti-biofilm patches. The scale bar is 500 nm.

3.5. Implementability and scale-up considerations for proposed catalytic/ reactive membrane approach.

Scale-up considerations are particularly important in the current case due to the massive scale of implementation of RO/NF systems. As an example, the total current operating capacity of seawater RO plants is over 40 million m³/day [59] and plants as large as 330,000 m³/day have already been constructed [60]. Therefore, to keep the design of the proposed catalytic membrane and its operation simpler, in this work, currently used methods and materials were selected to minimize costs and other practical barriers to implementation.

H₂O₂ is already used for membrane cleaning at concentrations an order of magnitude higher than proposed in this work [33] and has a reasonable bulk cost of approximately \$0.50/lb [61] which is comparable in cost to the commonly used water treatment chemicals such as alum (\$0.96/lb) or sodium bisulfite (\$0.32/lb) [61].

In terms of operation, one of two approaches can be utilized to implement catalytic membrane operation without interrupting membrane filtration: 1) intermittent dosing of peroxide on a daily basis (4-6 hours) to remove deposited particles and relieve concentration polarization, or 2) continuous dosing of peroxide to prevent deposition of bacteria and colloids and to minimize concentration polarization throughout operation. The first approach would be more economical and perhaps more applicable to low fouling waters while the second approach could be more applicable to aggressively fouling water with high microbial and particle loads where concentration polarization is also challenging (due to high salinity and or high operating flux). Using a catalytic membrane and periodic H₂O₂ dosing, we estimated 19% specific energy savings (in terms of kwh/m³) over a period of 1 month in a typical high fouling low pressure RO system with 37% trans-membrane pressure increase (**Supplementary Information and Supplementary Fig. S8**). In a high-pressure RO system, assuming comparable fouling rate, we

estimated a dramatic increase in specific energy savings of 32% due to elimination of concentration polarization in addition to fouling mitigation.

The maximum stability of melanin like films (eg. polydopamine) was evaluated as 8 weeks by Bettinger *et al.* under in-vivo conditions [62]. In our experiments, we did not observe catalytic performance degradation during 7 days of experiments with multiple regeneration cycles (**Fig. 3e and Supplementary Fig. S3**). We propose two implementable pathways to regenerate the film or counter any degradation over time :

1. *Polymerization of dopamine in presence of hydroxyl radicals:* Chen *et al.* demonstrated that under acidic conditions, using hydroxyl radical rich plasma activated water (PAW), dopamine can be conveniently polymerized into polydopamine [63]. Interestingly, polydopamine is a self-healing polymer as it can be formed by polymerization under acidic, neutral and or basic conditions if reactive oxygen species are present [64]. Therefore, occasional addition of dopamine along with H_2O_2 might be an effective strategy to ensure longevity of the polydopamine film.
2. *Using poly(dopamine-ferrocene) composite polymer instead of only polydopamine:* Kumar *et al.* demonstrated that polymerization product of ferrocene modified dopamine is resistant to free radical attacks [65]. Therefore, using poly(dopamine-ferrocene) as the surface modification instead of mere polydopamine would increase the robustness of the coating layer and would minimize the requirement for frequent regeneration of such a layer.

In preliminary membrane integrity evaluations, there was no significant Rhodamine WT passage detected after using the catalytic membrane for 5 days under intermittent H₂O₂ addition (**Supplementary Information and Supplementary Table S3**) indicating that integrity was maintained under conditions tested in this work. The water permeability was also not affected in modifying the membrane, since the permeability ratio of virgin to modified membrane was 1.19±0.24 (**Supplementary Fig. S9**). In our studies, we did not detect any significant change in salt rejection with CuO/PDA catalytic membrane. For example, in concentration polarization experiments where intermittent H₂O₂ addition was performed, the initial and final NaCl rejections were 98.5% and 98.7%, respectively. In case of 50 ppm HA fouling elimination with 240 ppm H₂O₂ addition, the salt rejection was maintained at 98.6%, even after 5 days of continuous experiment. Additionally, we detected only 0.07 ppm Cu²⁺ in the recycled concentrate and less than 0.01 ppm Cu²⁺ (detection limit of method) in the permeate stream, after 24 h of 240 ppm H₂O₂ injection. Cu²⁺ likely accumulated in the system due to recycled mode of operation.

Modeling of the reaction kinetics revealed significant enrichment of the process water with molecular oxygen, which can be used to supplement the dissolved oxygen level as well as to minimize biochemical oxygen demand when discharged. However, the oxygen production rate stalled after consuming all H₂O₂ within ~2.5 h after charging (**Supplementary Information and Supplementary Fig. S10**). Therefore, opportunities exist to improve the process efficiency with continuous supply of H₂O₂ through *in-situ* generation by designing and developing novel catalysts [66].

4. CONCLUSIONS

Overall, we have presented an easily implementable, but effective approach to fouling mitigation by colloidal and organic foulants with additional advantage of biofilm control using a scalable surface modification of current membranes with nanoparticle catalysts. H₂O₂ addition to this system, reduces and completely eliminates concentration polarization, a first demonstration of this kind. Such an operational strategy in high-pressure membrane systems can reduce the energy expenditure substantially, particularly in sea water desalination where 70% of the operational cost is due to energy expenditure [59]. The proposed approach is also completely compatible with current membrane infrastructure and operational strategies without impeding regular operation.

ACKNOWLEDGMENTS

We thank Penn State College of Engineering ENGINE grant for funding this project. Funding from the National Science Foundation through the grant CBET - 1402063 and a CBET GOALI grant (CBET – 1705278) is also acknowledged. We also thank Penn State Agricultural Analytical Services Laboratory for helping in nanoparticle loading measurements.

ASSOCIATED CONTENT

Supporting Information

Supporting information includes experimental, materials and methods of synthesizing polydopamine-nanoparticle composite membranes, membrane characterization with methylene blue decolorization reaction, SEM and TEM, humic acid chelating behavior, methods of Rhodamine dye testing for membrane integrity, bubble generation and concentration

polarization, fouling behavior of CuO/ PDA membranes at different concentrations of H₂O₂, performance of MnO₂/ PDA membranes, theoretical modeling of bubble size and calculation of solute back diffusion mass transfer co-efficients under experimental conditions, estimation of energy savings with catalytic membranes, O₂ generation, dye rejection and permeability data. Supplementary data associated with this article can be found in the online version at <http://www.sciencedirect.com/science/journal/03767388>.

Supplementary video legend

Video S1. Methylene blue decolorization by catalytic bubble membrane 2 cm² of 80 ppm CuO/ PDA membrane decolorizes 12 ppm methylene blue with 3% H₂O₂. Bubble generation is observed with the active membrane at the right vial. In the control case without active membrane, no decolorization is noticed at the left vial. The movie spans total duration of 3 h.

REFERENCES

- [1] K. Vairavamoorthy, J. Herrick, L. Kauppi, J.A. Mcneely, J. Mcglade, E. Eboh, M. Smith, E. Acheampong, W. Pengue, A.B. Siriban-manalag, Options for decoupling economic growth from water use and water pollution, UNEP: Paris, 2016.
- [2] M.A. Shannon, P.W. Bohn, M. Elimelech, J.G. Georgiadis, B.J. Mariñas, A.M. Mayes, Science and technology for water purification in the coming decades, *Nature*. 452 (2008) 301–310.
- [3] R.K. McGovern, J.H. Lienhard V, On the potential of forward osmosis to energetically outperform reverse osmosis desalination, *J. Memb. Sci.* 469 (2014) 245–250.
- [4] J.R. Werber, C.O. Osuji, M. Elimelech, Materials for next-generation desalination and water purification membranes, *Nat. Rev. Mater.* 1 (2016) 16018.

- [5] F. Wang, V. Tarabara, Coupled effects of colloidal deposition and salt concentration polarization on reverse osmosis membrane performance, *J. Memb. Sci.* 293 (2007) 111–123.
- [6] M. Elimelech, W. a Phillip, The future of seawater desalination: energy, technology, and the environment., *Science.* 333 (2011) 712–717.
- [7] B. Culkin, Devise and Method for Filtering a Colloidal Suspension, US Patent 4952317, 1990.
- [8] R. Dashtpour, S.N. Al-zubaidy, Energy Efficient Reverse Osmosis Desalination Process, 3 (2012).
- [9] RO membranes and components market is growing at 10.5% CAGR, *Membr. Technol.* 2015 (2015) 4-.
- [10] M. Elimelech, X. Zhu, A.E. Childress, S. Hong, Role of membrane surface morphology in colloidal fouling of cellulose acetate and composite aromatic polyamide reverse osmosis membranes, *J. Memb. Sci.* 127 (1997) 101–109.
- [11] D. Rana, Y. Kim, T. Matsuura, H.A. Arafat, Development of antifouling thin-film-composite membranes for seawater desalination, *J. Memb. Sci.* 367 (2011) 110–118.
- [12] S. Yu, Z. Lü, Z. Chen, X. Liu, M. Liu, C. Gao, Surface modification of thin-film composite polyamide reverse osmosis membranes by coating N-isopropylacrylamide-co-acrylic acid copolymers for improved membrane properties, *J. Memb. Sci.* 371 (2011) 293–306.
- [13] H. Ju, B.D. McCloskey, A.C. Sagle, Y.-H. Wu, V.A. Kusuma, B.D. Freeman, Crosslinked poly(ethylene oxide) fouling resistant coating materials for oil/water separation, *J. Memb. Sci.* 307 (2008) 260–267.

- [14] G. Kang, Y. Cao, Development of antifouling reverse osmosis membranes for water treatment: A review, *Water Res.* 46 (2012) 584–600.
- [15] G. Trägårdh, Membrane cleaning, *Desalination.* 71 (1989) 325–335.
- [16] S.H. Kim, S.Y. Kwak, B.H. Sohn, T.H. Park, Design of TiO₂ nanoparticle self-assembled aromatic polyamide thin-film-composite (TFC) membrane as an approach to solve biofouling problem, *J. Memb. Sci.* 211 (2003) 157–165.
- [17] C.F. De Lannoy, D. Jassby, K. Gloe, A.D. Gordon, M.R. Wiesner, Aquatic biofouling prevention by electrically charged nanocomposite polymer thin film membranes, *Environ. Sci. Technol.* 47 (2013) 2760–2768.
- [18] H. Hachisuka, K. Ikeda, Reverse Osmosis Composite Membrane and Reverse Osmosis Treatment Method for Water Using the same, US Patent 6413425 B1, 2002.
- [19] T. Konishi, N. Kurata, K. Maruyama, Y. Uda, Y. Yamashiro, C. Harada, Composite Semipermeable Membranes and Process of Production thereof, US Patent Application 2010/0320143 A1, 2010.
- [20] S. Nishiyama, N. Kurata, T. Konishi, Y. Yamashiro, K. Maruyama, Y. Uda, C. Harada, Composite Semipermeable Membrane. US Patent 8672142 B2, 2014.
- [21] J.R. Ray, S. Tadepalli, S.Z. Nergiz, K.-K. Liu, L. You, Y. Tang, S. Singamaneni, Y.-S. Jun, Hydrophilic, Bactericidal Nanoheater-Enabled Reverse Osmosis Membranes to Improve Fouling Resistance, *ACS Appl. Mater. Interfaces.* (2015) 150519102300006.
- [22] W. Duan, A. Dudchenko, E. Mende, C. Flyer, X. Zhu, D. Jassby, Electrochemical mineral scale prevention and removal on electrically conducting carbon nanotube--polyamide reverse osmosis membranes., *Environ. Sci. Process. Impacts.* 16 (2014) 1300–8.
- [23] A. V. Dudchenko, J. Rolf, K. Russell, W. Duan, D. Jassby, Organic fouling inhibition on

- electrically conducting carbon nanotube-polyvinyl alcohol composite ultrafiltration membranes, *J. Memb. Sci.* 468 (2014) 1–10.
- [24] Y. Jing, L. Guo, B.P. Chaplin, Electrochemical impedance spectroscopy study of membrane fouling and electrochemical regeneration at a sub-stoichiometric TiO₂ reactive electrochemical membrane, *J. Memb. Sci.* 510 (2016) 510–523.
- [25] S.P. Chesters, M.W. Armstrong, M. Fazel, Microbubble RO membrane cleaning reduces fouling on WWRO plant, *Desalin. Water Treat.* 55 (2015) 2900–2908.
- [26] H.H. Himstedt, Q. Yang, L.P. Dasi, X. Qian, S.R. Wickramasinghe, M. Ulbricht, Magnetically Activated Micromixers for Separation Membranes, *Langmuir.* 27 (2011) 5574–5581.
- [27] B.D. McCloskey, H.B. Park, H. Ju, B.W. Rowe, D.J. Miller, B.D. Freeman, A bioinspired fouling-resistant surface modification for water purification membranes, *J. Memb. Sci.* 413–414 (2012) 82–90.
- [28] S. Kasemset, A. Lee, D.J. Miller, B.D. Freeman, M.M. Sharma, Effect of polydopamine deposition conditions on fouling resistance, physical properties, and permeation properties of reverse osmosis membranes in oil/water separation, *J. Memb. Sci.* 425–426 (2013) 208–216.
- [29] J. Jiang, L. Zhu, L. Zhu, H. Zhang, B. Zhu, Y. Xu, Antifouling and antimicrobial polymer membranes based on bioinspired polydopamine and strong hydrogen-bonded poly(*n* - vinyl pyrrolidone), *ACS Appl. Mater. Interfaces.* 5 (2013) 12895–12904.
- [30] R.X. Zhang, L. Braeken, P. Luis, X.L. Wang, B. Van der Bruggen, Novel binding procedure of TiO₂ nanoparticles to thin film composite membranes via self-polymerized polydopamine, *J. Memb. Sci.* 437 (2013) 179–188.

- [31] G. Cheng, S.-Y. Zheng, Construction of a high-performance magnetic enzyme nanosystem for rapid tryptic digestion, *Sci. Rep.* 4 (2014) 6947.
- [32] L. Tang, K.J.T. Livi, K.L. Chen, Polysulfone Membranes Modified with Bioinspired Polydopamine and Silver Nanoparticles Formed in Situ To Mitigate Biofouling, *Environ. Sci. Technol. Lett.* 2 (2015) 59–65.
- [33] Dow Water and Process Solutions, FILMTEC™ Reverse Osmosis Membranes Technical Manual. http://dowac.custhelp.com/app/answers/detail/a_id/3428/~/filmtec-membranes--filmtecs-technical-manual (accessed July 2016).
- [34] K. Feng, L. Hou, B. Tang, P. Wu, A self-protected self-cleaning ultrafiltration membrane by using polydopamine as a free-radical scavenger, *J. Memb. Sci.* 490 (2015) 120–128.
- [35] M. Lee, J. Rho, D.E. Lee, S. Hong, S.J. Choi, P.B. Messersmith, H. Lee, Water detoxification by a substrate-bound catecholamine adsorbent, *Chempluschem.* 77 (2012) 987–990.
- [36] D.P. Singh, A.K. Ojha, O.N. Srivastava, Synthesis of Different Cu(OH)₂ and CuO (Nanowires, Rectangles, Seed-, Belt-, and Sheetlike) Nanostructures by Simple Wet Chemical Route, *J. Phys. Chem. C.* 113 (2009) 3409–3418.
- [37] X. Lai, X. Li, W. Geng, J. Tu, J. Li, S. Qiu, Ordered Mesoporous Copper Oxide with Crystalline Walls, *Angew. Chemie - Int. Ed.* 46 (2007) 738–741.
- [38] S. Kanazawa, H. Kawano, S. Watanabe, T. Furuki, S. Akamine, R. Ichiki, T. Ohkubo, M. Kocik, J. Mizeraczyk, Observation of OH radicals produced by pulsed discharges on the surface of a liquid, *Plasma Sources Sci. Technol.* 20 (2011) 34010.
- [39] R. Guha, X. Shang, A.L. Zydney, D. Velegol, M. Kumar, Diffusiophoresis contributes significantly to colloidal fouling in low salinity reverse osmosis systems, *J. Memb. Sci.*

- 479 (2015) 67–76.
- [40] C.Y. Tang, Y.-N. Kwon, J.O. Leckie, Fouling of reverse osmosis and nanofiltration membranes by humic acid—Effects of solution composition and hydrodynamic conditions, *J. Memb. Sci.* 290 (2007) 86–94.
- [41] T.L. Wood, R. Guha, L. Tang, M. Geitner, M. Kumar, T.K. Wood, Living biofouling-resistant membranes as a model for the beneficial use of engineered biofilms, *Proc. Natl. Acad. Sci.* . 113 (2016) E2802–E2811.
- [42] M.H. Chen, S.S.S. Cardoso, The mixing of liquids by a plume of low-Reynolds number bubbles, *55* (2000) 2585–2594.
- [43] Experiments on Natural Transition in Separation Bubbles, *Procedia IUTAM.* 14 (2015) 496–502.
- [44] R.F. Tabor, R. Manica, D.Y.C. Chan, F. Grieser, R.R. Dagastine, Repulsive van der Waals Forces in Soft Matter: Why Bubbles Do Not Stick to Walls, *Phys. Rev. Lett.* 106 (2011) 64501.
- [45] C. Bohling, W. Sigmund, Repulsive van der Waals Forces Self-Limit Native Oxide Growth, *Langmuir.* 31 (2015) 4862–4867.
- [46] W. Pan, G. Zhang, T. Zheng, P. Wang, Degradation of p-nitrophenol using CuO/Al₂O₃ as a Fenton-like catalyst under microwave irradiation, *RSC Adv.* 5 (2015) 27043–27051.
- [47] D.R. Lovley, J.D. Coates, E.L. Blunt-Harris, E.J.P. Phillips, J.C. Woodward, Humic substances as electron acceptors for microbial respiration, *Nature.* 382 (1996) 445–448.
- [48] P. Liao, Y. Al-Ani, Z. Malik Ismael, X. Wu, Insights into the Role of Humic Acid on Pd-catalytic Electro-Fenton Transformation of Toluene in Groundwater, *Sci. Rep.* 5 (2015) 9239.

- [49] R.H. Liu, J. Yang, M.Z. Pindera, M. Athavale, P. Grodzinski, Bubble-induced acoustic micromixing., *Lab Chip*. 2 (2002) 151–7.
- [50] D. Velegol, A. Garg, R. Guha, A. Kar, M. Kumar, Origins of concentration gradients for diffusiophoresis, *Soft Matter*. (2016).
- [51] G. Almendros, F. Martín, F.J. González-Vila, Depolymerization and degradation of humic acids with sodium perborate, *Geoderma*. 39 (1987) 235–247.
- [52] D.A. Ladner, A. Subramani, M. Kumar, S.S. Adham, M.M. Clark, Bench-scale evaluation of seawater desalination by reverse osmosis, *Desalination*. 250 (2010) 490–499.
- [53] E.M. V Hoek, M. Elimelech, Cake-Enhanced Concentration Polarization: A New Fouling Mechanism for Salt-Rejecting Membranes, *Environ. Sci. Technol*. 37 (2003) 5581–5588.
- [54] A.L. Zydney, Stagnant film model for concentration polarization in membrane systems, *J. Memb. Sci*. 130 (1997) 275–281.
- [55] J. Abraham, K.S. Vasu, C.D. Williams, K. Gopinadhan, Y. Su, C.T. Cherian, J. Dix, E. Prestat, S.J. Haigh, I. V Grigorieva, P. Carbone, A.K. Geim, R.R. Nair, Tunable sieving of ions using graphene oxide membranes, *Nat Nano. advance on* (2017).
- [56] D. Cohen-Tanugi, R.K. McGovern, S.H. Dave, J.H. Lienhard, J.C. Grossman, Quantifying the potential of ultra-permeable membranes for water desalination, *Energy Environ. Sci*. 7 (2014) 1134–1141.
- [57] C. Gunawan, W.Y. Teoh, C.P. Marquis, R. Amal, Cytotoxic Origin of Copper(II) Oxide Nanoparticles: Comparative Studies with Micron-Sized Particles, Leachate, and Metal Salts, *ACS Nano*. 5 (2011) 7214–7225.
- [58] J. Cui, Y. Ju, K. Liang, H. Ejima, S. Lörcher, K.T. Gause, J.J. Richardson, F. Caruso,

- Nanoscale engineering of low-fouling surfaces through polydopamine immobilisation of zwitterionic peptides., *Soft Matter*. 10 (2014) 2656–63.
- [59] L.K. Wang, J.P. Chen, Y.-T. Hung, N.K. Shammam, *Membrane and desalination technologies*, Springer, 2010.
- [60] B. Sauvet-Goichon, EuroMed 2006 Ashkelon desalination plant — A successful challenge, *Desalination*. 203 (2007) 75–81.
- [61] Independent Chemical Information Service Indicative Chemical Prices.
<http://www.icis.com/chemicals/channel-info-chemicals-a-z/> (accessed July 2016).
- [62] C.J. Bettinger, J.P. Bruggeman, A. Misra, J.T. Borenstein, R. Langer, Biocompatibility of biodegradable semiconducting melanin films for nerve tissue engineering, *Biomaterials*. 30 (2009) 3050–3057.
- [63] T.-P. Chen, T. Liu, T.-L. Su, J. Liang, Self-Polymerization of Dopamine in Acidic Environments without Oxygen, *Langmuir*. 33 (2017) 5863–5871.
- [64] X. Du, L. Li, J. Li, C. Yang, N. Frenkel, A. Welle, S. Heissler, A. Nefedov, M. Grunze, P.A. Levkin, UV-Triggered Dopamine Polymerization: Control of Polymerization, Surface Coating, and Photopatterning, *Adv. Mater.* 26 (2014) 8029–8033.
- [65] T.N. Kumar, S. Sivabalan, N. Chandrasekaran, K.L.N. Phani, Ferrocene-functionalized polydopamine as a novel redox matrix for H₂O₂ oxidation, *J. Mater. Chem. B*. 2 (2014) 6081.
- [66] Y. Shiraishi, S. Kanazawa, Y. Kofuji, H. Sakamoto, S. Ichikawa, S. Tanaka, T. Hirai, Sunlight-driven hydrogen peroxide production from water and molecular oxygen by metal-free photocatalysts, *Angew. Chemie - Int. Ed.* 53 (2014) 13454–13459.

Highlights

- O₂ evolving reactive RO membrane was tested in high pressure crossflow filtration
- Eliminated colloidal and organic fouling using bubble induced reactive micromixing
- Eliminated concentration polarization by micromixing enhanced solute back diffusion
- *E. coli*. biofilm formation was substantially reduced due to anchored CuO nanoparticles

Accepted manuscript